Two-Compartment Models of the Diffusion MR Signal in Brain White Matter

Eleftheria Panagiotaki[1], Hubert Fonteijn[1], Bernard Siow[1,2], Matt G. Hall[1], Anthony Price[2], Mark F. Lythgoe[2], and Daniel C. Alexander[1,⋆]

[1] Centre for Medical Image Computing, Department of Computer Science, University College London, UK
E.Panagiotaki@cs.ucl.ac.uk
[2] Centre for Advanced Biomedical Imaging , University College London, UK

Abstract. This study aims to identify the minimum requirements for an accurate model of the diffusion MR signal in white matter of the brain. We construct a hierarchy of two-compartment models of white matter from combinations of simple models for the intra and extra-cellular spaces. We devise a new diffusion MRI protocol that provides measurements with a wide range of parameters for diffusion sensitization both parallel and perpendicular to white matter fibres. We use the protocol to acquire data from a fixed rat brain, which allows us to fit, study and compare the different models. The results show that models which incorporate pore size describe the measurements most accurately. The best fit comes from combining a full diffusion tensor (DT) model of the extra-cellular space with a cylindrical intra-cellular component.

1 Introduction

Over the last 15 years diffusion-weighted MRI (DW-MRI) has become popular because it provides unique insight into brain tissue microstructure and connectivity. The technique has become an essential probe for highlighting and monitoring tissue microstructure changes in development and disease.

The simplest and most commonly used model for relating the DW-MRI signal to diffusion in tissue is the diffusion tensor (DT) [1]. The model provides useful microstructural markers of tissue integrity such as fractional anisotropy (FA) and mean diffusivity (MD). However these indicators are non-specific, because many features of the microstructure can affect them. To address this limitation, the recent trend in diffusion MRI [2,3,4] is towards more direct microstructure imaging via more descriptive models of tissue that relate specific parameters, such as cell size and density, directly to the signal.

To trust the parameter estimates we obtain from fitting these models, we must ensure that they include all the important physiological parameters of the tissue

⋆ Thanks to Mankin Choy and Johannes Riegler for help with the sample preparation. Funded by EPSRC grants EP/E056938/1 and EP/E007748, British Heart Foundation and BBSRC.

G.-Z. Yang et al. (Eds.): MICCAI 2009, Part I, LNCS 5761, pp. 329–336, 2009.

that affect the signal. In this work, we study one important class of models: two-compartment models with no exchange, which model the signal as the sum of signals from water inside and outside impermeable cells. The class of models includes the ball and stick model [2], CHARMED [4] and the simplified version of CHARMED in [3], each of which uses different intra-cellular (IC) and extra-cellular (EC) models. We construct a hierarchy of two-compartment models from combinations of these IC and EC models. We define a new diffusion MRI protocol to allow evaluation and comparison of the models for parallel and perpendicular signals in brain white matter over a wide range of scan parameters. Such a study is challenging in brain tissue because fibre orientation varies, so most previous studies use simpler tissue samples such as spinal cord. The new protocol enables extension of these studies to the brain. Here we acquire data from an ex vivo rat brain that has been perfusion fixed. The data set contains a much more comprehensive set of measurements than we can acquire on live subjects but is rich enough to ensure good fit of the models, identification of important effects and thus reliable selection of appropriate models for sparser in vivo data.

Section 2 gives some background on diffusion MRI models. Section 3 introduces the hierarchy of models to test, the MRI acquisition protocol and the model fitting procedure. Section 4 describes the experiments and results.

2 Background

Diffusion tensor imaging (DTI) [1] models the displacement of spins in 3D with a zero-mean Gaussian distribution by fitting the apparent diffusion tensor $\mathbf{D}$, to six or more normalised DW images via

$$S(\mathbf{G}, \Delta, \delta) = S_0 \exp(-b\hat{\mathbf{G}}^T \mathbf{D} \hat{\mathbf{G}}), \tag{1}$$

where S is the DW signal, S_0 is the unweighted signal, b is the diffusion weighting factor, equal to $(\Delta - \delta/3)(\gamma\delta|\mathbf{G}|)^2$ for the pulse-gradient spin-echo (PGSE) sequence , $\mathbf{G}$ is the gradient vector with strength $|\mathbf{G}|$ and direction $\hat{\mathbf{G}}$, Δ is the time between the onsets of the two pulses, δ is the pulse gradient duration and γ is the gyromagnetic ratio. A big limitation of the DT model is that it does not account for restricted diffusion within cells so the signal departs from the model even in single fibre populations especially as b becomes large.

Two-compartment models overcome the limitations of the DT model to some extent by modelling restriction within cells. Often they assume hindered diffusion in the EC space and restricted diffusion in the IC space. The signal attenuation is given by

$$S(\mathbf{G}, \Delta, \delta) = S_0 \Big(f S_h(\mathbf{G}, \Delta, \delta) + (1 - f) S_r(\mathbf{G}, \Delta, \delta) \Big), \tag{2}$$

where f is the volume fraction of the restricted IC compartment, S_h and S_r are signals from the hindered and the restricted compartments respectively.

In Behrens' ball and stick model [2] both S_r and S_h have the form of Eq. 1. For S_r, $\mathbf{D} = d\mathbf{n}\mathbf{n}^T$ where d is the free diffusivity and $\mathbf{n}$ is the fibre direction, so water moves only in the fibre direction. For S_h, $\mathbf{D} = d\mathbf{I}$, where $\mathbf{I}$ is the identity tensor, so diffusion is isotropic.

Alexander [3] models the EC space using Eq. 1 with a cylindrically symmetric tensor, so $\mathbf{D} = \alpha\mathbf{n}\mathbf{n}^T + \beta\mathbf{I}$. The model for the IC space accounts for non-zero pore size, unlike Behrens' stick model. S_r comes from Van Gelderen's model [5] for signal attenuation from diffusion perpendicular to the axis of a restricting cylinder and accounts for finite pulse width.

Assaf's CHARMED model [4] also assumes cylindrical restriction in the IC space. They use Neuman's expression [6] for diffusion in cylindrical confinement for a PGSE experiment, which assumes short gradient pulses ($\delta \ll \Delta$). Unlike Alexander's model, which assumes a single cylinder radius, the model assumes cylinders with gamma distributed radii which introduces one extra parameter. The hindered compartment uses the full DT model constrained only to have principal direction aligned with the cylinder axis.

Other methods describe diffusion with three or more compartments and allow exchange between them. For example, Stanisz et al. [7] construct a three-pool model with prolate ellipsoidal axons and spherical glial cells each with partially permeable membranes. However, fitting such models requires very high quality measurements, typically using NMR spectroscopy rather than MRI. We limit investigation here to simpler two-compartment models with no exchange.

3 Methods

This section describes the hierarchy of two-compartment models, the details of the new acquisition protocol and the model fitting procedure.

3.1 Model Hierarchy

There are many options in the literature for models of the S_r and S_h components from which we can combine any pair to create new two-compartment models.

We investigate two models for the restricted compartment. The first is Behrens' "stick" model [2] which has $\mathbf{n}$ and d as parameters. This describes diffusion in a zero radius cylinder. The second is Van Gelderen's model [5], as used in [3], which accounts for non-zero cylinder radius. We refer to this model as the "cylinder". This model has an extra parameter, R, the axon radius. We assume a single R as in [3].

We investigate three models for the EC compartment. Each is a DT model with different constraints. The first, the "ball", is isotropic, $\mathbf{D} = d\mathbf{I}$, as in [2] and has only one parameter, the diffusivity d. The second has a DT which is anisotropic, but cylindrically symmetric, as in [3] and we call this a "zeppelin". The model has parameters: $\mathbf{n}$, $d_\parallel$ which is the diffusivity parallel to the fibre direction and $d_\perp$ perpendicular to it.

Finally we consider a full tensor. This model has three diffusivity parameters: parallel diffusivity $d_\parallel$ and $d_{\perp_1}$,$d_{\perp_2}$ perpendicular with $d_{\perp_1} \neq d_{\perp_2}$. It has an additional three degrees of freedom for the orthogonal eigenvectors $\mathbf{n}$, $\mathbf{n}_{\perp_1}$ and $\mathbf{n}_{\perp_2}$. The form of the DT is

$$\mathbf{D}_h = d_\parallel \mathbf{n}\mathbf{n}^T + d_{\perp_1}\mathbf{n}_{\perp_1}\mathbf{n}_{\perp_1}^T + d_{\perp_2}\mathbf{n}_{\perp_2}\mathbf{n}_{\perp_2}^T. \quad (3)$$

We refer to this EC model as a "boat". We use combined terms to refer to specific two-compartment models, for example "zeppelin and stick" assumes zero radius cylinders for the IC space and cylindrical symmetry for the EC space. Where appropriate we further constrain the EC models so that the DT's principal direction is equal to the IC cylinder axis and the EC diffusivity is $d_{\|}$.

3.2 MRI Acquisition

We are interested in diffusion in the brain in directions parallel and perpendicular to the fibre orientation, since these directions reveal most about the underlying brain microstructure. However, it is challenging to acquire such measurements from brain tissue, because fibre orientation varies throughout the white matter. Our approach is to pick one central parallel direction and several perpendicular directions and identify voxels in which the fibres align with those directions after imaging. We focus analysis only on these voxels and discard all others.

We acquire diffusion-weighted MR images of a perfusion-fixed male rat brain, using a small bore 9.4T scanner (Varian) with maximum gradient strength 400 mT/m. We use a five direction-encoding scheme and place the sample in the scanner oriented to ensure that some fibres in the Corpus Callosum (CC) are parallel to our central direction. We choose four evenly spaced directions perpendicular to the central direction in our chosen voxels (see Figure 1). We use a PGSE sequence for 70 diffusion weightings: five diffusion times Δ = 10, 20, 30, 40, 50 ms, gradient durations δ = 3 ms for all Δ and δ = 30 ms for Δ = 40, 50 ms, gradient strength $|\mathbf{G}|$ varied from 40 to 400 mT/m in ten steps of 40 mT/m. Measurements with b value greater than $7.7 \times 10^{10}\,\mathrm{sm}^{-2}$ were not performed due to poor SNR (< 2.6 i.e all combinations with $|\mathbf{G}| = 200$ to 400 mT/m and $\delta = 30$ ms). In total we acquired images with 59 diffusion weightings in each direction. In figure 2 we plot the parallel and the mean of the four perpendicular directions of the log signal from voxels in the region of interest (see section 4) in the CC and demonstrate MRI images for various b values.

We use minimum echo times (TE) to maximise SNR and repetition times (TR) to minimise gradient heating effects. For each combination of diffusion weighting parameters we acquire $b = 0$ images to correct for T1 and T2 dependence. We also perform a separate DTI acquisition using a 42-direction scheme with b value $4.5 \times 10^{9}\,\mathrm{sm}^{-2}$ and six $b = 0$ measurements. The in-plane field of view is 2 cm, matrix size 256×256 and slice thickness 0.5 mm.

3.3 Model Fitting

We fit each model to the data using an iterative optimization procedure and synthesise diffusion-weighted data from the fitted models. We minimize the sum of squared errors using a Levenberg-Marquardt algorithm. Fits of the simplest models are relatively independent of starting position. More complex models are more sensitive and we use parameter estimates of simpler models to provide initial estimates. We choose the best fit parameters from the models after 500 perturbations of the starting parameters to ensure a good minimum. Fitting procedures are implemented in Camino [8].

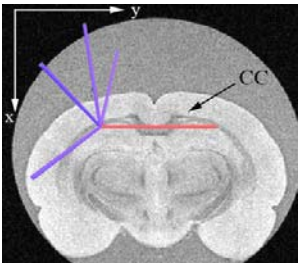

Fig. 1. The red arrow indicates the central gradient direction used for the encoding scheme and the blue arrows indicate the four directions perpendicular to the central one

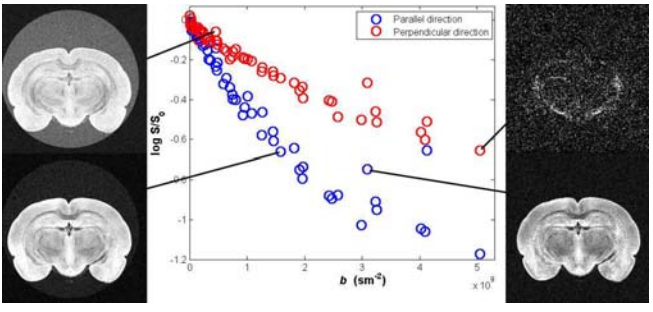

Fig. 2. Plot of the parallel and the mean of the four perpendicular directions of the log signal from voxels in a region of interest in the CC and demonstration of MRI images for various b values

4 Experiments and Results

To study parallel and perpendicular signal attenuation we choose a region of interest (ROI) with fibre direction aligned to the central direction. We manually segment the CC on a FA map from the DTI acquisition and threshold for voxels with FA > 0.5 in which the principal direction of the DT is parallel to the central gradient direction within $2\,^{\circ}$. We average the data contained within all the resulting 21 voxels of the ROI.

The best fit microstructure parameters from the models are shown in table 1. We see that the "cylinder" models give higher values for the volume fraction f and diffusivity parameters and consistently estimate R around $2\,\mu$m, which is a reasonable estimate of mean axon radius. All the models give good estimates of the left-right fibre direction.

The Bayesian information criterion (BIC) [9] evaluates the models and accounts for varying complexity. Table 2 shows the mean-squared error (MSE) and BIC for all the models. As expected, MSE decreases with model complexity, but the BIC reveals which reductions are significant. The "boat and cylinder" model minimizes the BIC.

Figure 3 shows the fit of each model to the data. The top right panel shows scan data and the other panels compare predictions from each model with fitted parameters. The plots actually show the mean signals over 500 trials adding independent Rician noise at approximately the level in the scan data. This procedure

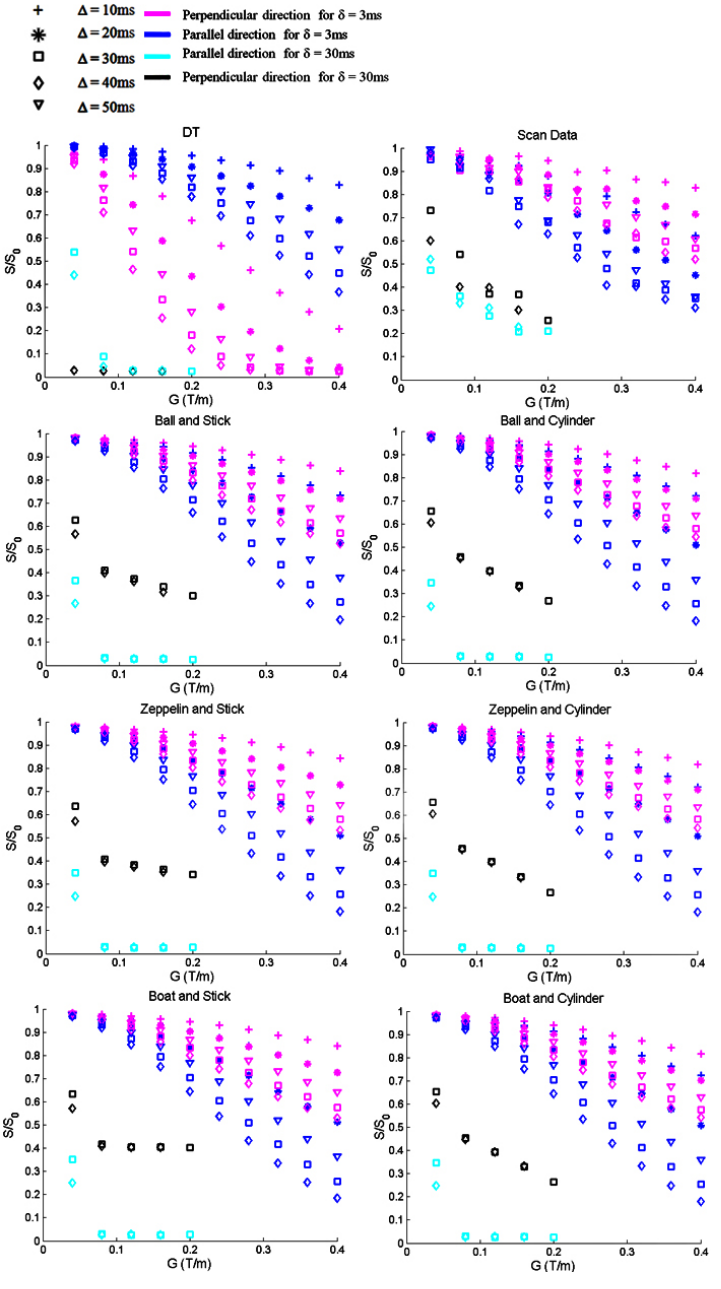

Fig. 3. Results of data synthesised from the analytical models and the scan data from the PGSE experiment. The normalised signal S/S_0 is plotted for all the values of Δ, δ as a function of the gradient strength $|\mathbf{G}|$ for the parallel and the mean of the four perpendicular directions.

only significantly affects the measurements with very low signal. We compare data synthesised from the models by plotting the normalised signal S/S_0 at all values of Δ and δ as a function of the gradient strength $\mathbf{G}$ for the parallel and perpendicular directions. The DT model shows a significant departure from the scan data and confirms expectations that the model is poor for high b value data, because it does not account for restriction. In contrast, all the two-compartment models capture the broad trends of the data and the anisotropy that separates the parallel and perpendicular signals. The subtle variations that improve the fit for cylinder and anisotropic models are difficult to observe qualitatively.

Table 1. Fitted parameters for each model

Models	f	$d_{\parallel}$ ($\mathrm{m^2 s^{-1}}$)	$d_{\perp_1}$ ($\mathrm{m^2 s^{-1}}$)	$d_{\perp_2}$ ($\mathrm{m^2 s^{-1}}$)	R (m)	θ	φ
DT	n/a	2.494×10^{-11}	1.781×10^{-11}	1.660×10^{-11}	n/a	1.570	4.712
Ball and stick	0.429	3.211×10^{-10}	n/a	n/a	n/a	1.570	4.712
Ball and cylinder	0.503	3.389×10^{-10}	n/a	n/a	2.058×10^{-6}	1.518	4.753
Zeppelin and stick	0.408	3.3676×10^{-10}	2.914×10^{-10}	n/a	n/a	1.491	4.790
Zeppelin and cylinder	0.503	3.387×10^{-10}	3.396×10^{-10}	n/a	2.059×10^{-6}	1.518	4.754
Boat and stick	0.410	3.363×10^{-10}	3.772×10^{-10}	2.179×10^{-10}	n/a	1.682	4.704
Boat and cylinder	0.499	3.381×10^{-10}	4.442×10^{-10}	2.405×10^{-10}	2.101×10^{-6}	1.579	4.707

Models	MSE $\times10^4$	BIC $\times10^{-3}$	No. parameters
DT	1025.4	-0.7651	7
Ball and stick	34.5	-1.9768	5
Ball and cylinder	30.8	-2.0116	6
Zeppelin and stick	33.3	-1.9832	6
Zeppelin and cylinder	30.8	-2.0058	7
Boat and stick	30.3	-2.0051	8
Boat and cylinder	27.4	-2.0349	9

Table 2. Mean-squared fitting error, Bayesian information criteria and the number of parameters (with S_0) for each model

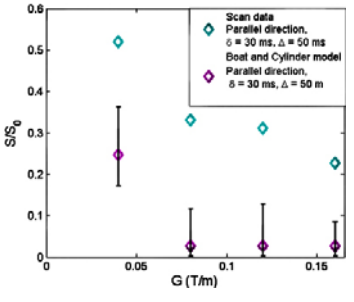

Fig. 4. Plot of the normalised signal for the parallel direction at $\delta = 30\,\mathrm{ms}$ and $\Delta = 50\,\mathrm{ms}$ from the scan data and the "boat and cylinder" model against the gradient strength. The error bars indicate the minimum and maximum signal over 500 Rician noise trials

The biggest departures are for large δ in the parallel direction. We hypothesise that these departures are not solely due to noise. Figure 4 compares the normalised signal S/S_0 for the scan data and the "boat and cylinder" model with $\delta = 30\,\mathrm{ms}$ and $\Delta = 50\,\mathrm{ms}$ for the parallel direction indicating the range of Rician noise over 500 realisations, confirming this.

5 Conclusions

We have constructed, evaluated and compared a hierarchy of two-compartment models for the DW-MRI signal in white matter. Previous studies of this type [4,7] have been limited to non-brain tissue, such as spinal cord or nerve tissue samples, because of the difficulty of obtaining parallel and perpendicular measurements

consistently from the brain. The new imaging protocol we devise provides parallel and perpendicular signals from brain tissue.

The models we present here are applicable and feasible for whole-brain imaging but the acquisition protocol is purposefully not. The aim of this work is to compare models with fixed orientation, which allows many more measurements to support the model comparison. Once we have established appropriate models, subsequently we can find more economical protocols for whole-brain imaging, using for example the ideas in [3].

The key conclusion is that the effects of restriction are extremely important for modelling diffusion in white matter. The simple two-compartment models we study here explains the data remarkably well. Even the simplest four-parameter (excluding S_0) ball and stick model captures the broad trends in the data where the six-parameter DT model completely fails. The model comparison in table 2 clearly demonstrates that the data supports the non-zero axon radius parameter, adding credence to techniques that estimate the parameter [3,4,7], as well as anisotropy of the EC compartment. The departure of the signals from the model in the parallel direction most likely comes from a small amount of restriction parallel to the fibres from glial cells and/or non-parallel fibres, which supports Stanisz's findings in [7], or from effects of tissue fixation.

Future work will extend the hierarchy to other IC and EC models and compare models that include exchange between compartments and different diffusivity and relaxivity in each compartment, as in [7]. In particular, we could include the gamma distribution model of the cylinder radii in [4]. The imaging protocol and methods we use here extend easily to support comparisons of an extended hierarchy of models.

References

1. Basser, P.J., Mattiello, J., LeBihan, D.: MR diffusion tensor spectroscopy and imaging. Biop J. 66, 259–267 (1994)
2. Behrens, T.E.J., Woolrich, M.W., Jenkinson, M., Johansen, H.: Characterization and propagation of uncertainty in diffusion-weighted MR imaging. Magn. Reson. Med. 50, 1077–1088 (2003)
3. Alexander, D.C.: A general framework for experiment design in diffusion MRI and its application in measuring direct tissue-microstructure features. Magn. Reson. Med. 60, 439–448 (2008)
4. Assaf, Y., Basser, P.: Composite hindered and restricted model of diffusion (CHARMED) MR imaging of the human brain. NeuroImage 27, 48–58 (2005)
5. Gelderen, P.V., Despres, D., Zijl, P.C.M.V., Moonen, C.T.W.: Evaluation of restricted diffusion in cylinders phosphocreatine in rabbit leg muscle. J. Magn. Reson. Series B 103, 255–260 (1994)
6. Neuman, C.H.: Spin echo of spins diffusing in a bounded medium. J. Chem. Phys. 60, 4508–4511 (1974)
7. Stanisz, G.J., Szafer, A., Wright, G.A., Henkelman, R.M.: An analytical model of restricted diffusion in bovine optic nerve. Magn. Reson. Med. 37, 103–111 (1997)
8. Cook, P.A., Bai, Y., Nedjati-Gilani, S., Seunarine, K.K., Hall, M.G., Parker, G.J., Alexander, D.C.: Camino: Open source diffusion- MRI reconstruction and processing. In: Proc. 14th Meeting of ISMRM, Seattle, WA, USA, vol. 2759 (2006)
9. Schwarz, G.: Estimating the dimension of a model. Ann. Stat. 6, 461–464 (1978)